9-6-2021

Comparison of Theoretical and Multi-Fidelity Optimum Aerostructural Solutions for Wing Design

Jeffrey D. Taylor
Utah State University

Douglas F. Hunsaker
Utah State University, doug.hunsaker@usu.edu

Recommended Citation

Taylor, J. D. and Hunsaker, D. F., "Comparison of Theoretical and Multi-Fidelity Optimum Aerostructural Solutions for Wing Design," Journal of Aircraft, Vol. 59, No. 1, Jan-Feb 2022, pp. 103-116. doi.org/10.2514/1.C036374

Comparison of Theoretical and Multi-Fidelity Optimum Aerostructural Solutions for Wing Design

Jeffrey D. Taylor* and Douglas F. Hunsaker†
Utah State University, Logan, Utah 84322-4130

As contemporary aerostructural research for aircraft design trends toward high-fidelity computational methods, aerostructural solutions based on theory are often neglected or forgotten. In fact, in many modern aerostructural wing optimization studies, the elliptic lift distribution is used as a benchmark in place of theoretical aerostructural solutions with more appropriate constraints. In this paper, we review several theoretical aerostructural solutions that could be used as benchmark cases for wing design studies, and we compare them to high-fidelity solutions with similar constraints. Solutions are presented for studies with 1) constraints related to the wing integrated bending moment, 2) constraints related to the wing root bending moment, and 3) structural constraints combined with operational constraints related to either wing stall or wing loading. It is shown that for each set of design constraints, the theoretical optimum lift distribution is consistently in excellent agreement with high-fidelity results. It follows that theoretical optimum lift distributions can often serve as a good benchmark for higher fidelity aerostructural wing optimization methods. Moreover, a review of solutions for the optimum wingspan and corresponding drag reveals important insights into the effects of viscosity, aeroelasticity, and compressibility on the aerodynamic and structural coupling involved in wing design and optimization.

Nomenclature

A = beam cross-sectional area

B_n = Fourier coefficients in the lifting-line solution for the dimensionless section-lift distribution

b = wingspan

* PhD Candidate, Mechanical and Aerospace Engineering, 4130 Old Main Hill, AIAA Student Member
† Assistant Professor, Mechanical and Aerospace Engineering, 4130 Old Main Hill, AIAA Senior Member

C_D = global drag coefficient

C_L = global lift coefficient

$\widetilde{C}_{L_{\max}}$ = maximum lift coefficient of the local airfoil section

C_δ = shape coefficient for the deflection-limited design, Eq. (5)

C_σ = shape coefficient for the stress-limited design, Eq. (4)

c = local wing section chord length

D = total drag

D_i = induced drag

D_{ref} = reference drag

E = modulus of elasticity of the beam material

h = height of the beam cross-section

I = beam section moment of inertia

J = aerostructural cost function based on a linear combination of drag and weight

L = total lift

$\widetilde{L}$ = local wing section lift

$\widetilde{M}_b$ = local wing section bending moment

n_a = load factor, g

n_g = limiting load factor at the hard-landing design limit

n_m = limiting load factor at the maneuvering-flight design limit

R_T = wing taper ratio

$s_{g,TO}$ = takeoff ground roll

$s_{g,L}$ = landing ground roll

S_b = proportionality coefficient between $\widetilde{W}_s(y)$ and $\widetilde{M}_b(y)$ having units of length squared

S_W = wing planform area

T = thrust

t_f = landing brake-engagement reaction time

t_r = takeoff rotation time

$t_{\max}$ = maximum thickness of the local airfoil section

V_{stall} = stall speed

V_∞ = freestream airspeed

W = aircraft gross weight

W_n = aircraft net weight, defined as $W - W_s$

W_s = total weight of the wing structure required to support the wing bending-moment distribution

W_{ref} = reference weight

$\widetilde{W}_n$ = net weight of the wing per unit span, i.e., total wing weight per unit span less $\widetilde{W}_s$

$\widetilde{W}_s$ = weight of the wing structure per unit span required to support the wing bending-moment distribution

y = spanwise coordinate relative to the midspan

β = relative weighting coefficient in the linear combination of drag and weight

γ = specific weight of the beam material

$\delta_{\max}$ = maximum wing deflection

μ_r = coefficient of rolling friction between the aircraft landing gear and the ground

ρ = air density

$\sigma_{\max}$ = maximum longitudinal stress

I. Introduction

Much of our current understanding of finite-wing design is based on solutions obtained from early analytic theories. Designers often rely on insights gained from these theories in the conceptual and preliminary phases of

aircraft design. In many cases, solutions based on theory have been shown to be in good agreement with experimental data and computational fluid dynamics [1-8], while providing significantly more mathematical and physical insight than higher fidelity models. In some cases, the applicability of a theoretical solution extends far beyond the assumptions and approximations associated with the original theory. For example, the well-known elliptic lift distribution was first identified in 1918 by Prandtl [9,10] and later by Munk [11] from analytic solutions based on lifting-line theory [9,10]. Within the approximations associated with lifting-line theory, the elliptic lift distribution minimizes induced drag on an unswept planar wing with fixed weight and wingspan. Since 1918, the elliptic lift distribution has appeared repeatedly in analytic, computational, and experimental studies, and it has been shown to be optimal for many complex and unconventional wing designs in both high- and low-speed subsonic flight. Therefore, the elliptic lift distribution is often used as a benchmark in many multi- and high-fidelity aerodynamic studies. Still, the elliptic lift distribution is only optimal under a limited set of aerodynamic design constraints [12-21].

When aerostructural constraints are considered, induced drag is typically minimized using a non-elliptic lift distribution [22-32] that depends on the tradeoff between the weight, wingspan, and lift distribution. Prandtl's classical lifting-line theory [9,10] provides insights about this tradeoff. From classical lifting-line theory, the induced drag D_i on a wing in steady-level flight with freestream density ρ and freestream velocity V_∞ can be written as

$$D_i = \frac{2(W/b)^2}{\pi\rho V_\infty^2}\left(1+\sum_{n=2}^{\infty} nB_n^2\right) \tag{1}$$

where W is the weight, b is the wingspan, and B_n are Fourier coefficients that define the lift distribution. When weight and wingspan are fixed, Eq. (1) is minimized with the elliptic lift distribution, which has $B_n = 0$ for all n. If the weight and wingspan are allowed to vary, Eq. (1) can be reduced by decreasing the weight and/or increasing the wingspan. However, this cannot be done arbitrarily because the wingspan, lift distribution, and weight are all coupled through the bending moments. Certain non-elliptic lift distributions can alleviate bending moments, allowing a larger wingspan with little or no increase in wing weight. Thus, the solution found by minimizing Eq. (1) with variable weight and/or wingspan often includes a non-elliptic lift distribution that is the aerostructural analogue of the aerodynamically-optimum elliptic lift distribution.

Early literature includes many theoretical and analytic studies that highlight these aerostructural tradeoffs and give solutions for the optimum lift distribution, wingspan, and in some cases wing weight, that minimize induced drag [33-43]. For example, in 1933, Prandtl identified a bell-shaped lift distribution that minimizes induced drag on a rectangular wing with fixed gross weight and moment of inertia of gross weight [33]. Independently, Jones [34] sought to minimize induced drag under the constraints of fixed gross lift and root bending moment in cruise. Pate and German [35] constrained the root bending moment at a given off-design lift coefficient but did not allow the wingspan to change. DeYoung [36] used a constraint on the bending moment at a prescribed spanwise location. Following Prandtl's lead [33], Jones and Lasinski [37] sought to minimize induced drag on non-planar wings with constrained integrated bending moment. Klein and Viswanathan [38,39] considered both root and integrated bending moment [38] and included the effects of shear on the wing-structure weight [39]. Extending Prandtl's [33] and Jones and Lasinski's [37] structural constraints, Löbert [40] introduced a constraint based on the ratio of the bending-moment distribution and the wing-section thickness. More recently, Phillips et al. [41,42] and Taylor and Hunsaker [43] extended Prandtl's approach [33] to account for the effects of the planform shape and the wing weight distribution and identified lift distributions that minimize induced drag under constraints of fixed gross weight [41], fixed net weight [42,43], fixed wing loading [41-43], and fixed stall speed [42].

Like most theoretical studies, each of these studies includes assumptions and approximations that are not fully representative of all aircraft wings, particularly those with unconventional designs. In part because of this, recent research in aerostructural design and optimization has trended toward developing high-fidelity computational methods that can handle complex geometries and design conditions. Theoretical aerostructural solutions are seldom revisited, and some are neglected or forgotten altogether. In fact, in the modern aerostructural literature, the elliptic lift distribution is often included as a benchmark [22-25,44,46-48] instead of theoretical aerostructural solutions with more applicable constraints. Yet, as is the case for the aerodynamically-optimum elliptic lift distribution, theoretical aerostructural solutions may have value well beyond their original assumptions and many may serve as appropriate benchmarks for higher fidelity studies.

In this paper, we address two questions: 1) How well do theoretical aerostructural solutions apply to typical real-world aircraft configurations? and 2) Can theoretical aerostructural solutions serve as an appropriate benchmark for higher fidelity studies? We address these questions by reviewing solutions from several theoretical aerostructural

studies [33,34,36-43] and comparing their solutions for the optimum lift distribution, wingspan, and drag to results from several multi- and high-fidelity computational studies on various practical aircraft configurations with comparable constraints [44-46,49-61]. Results are also compared to the elliptic lift distribution. As will be shown, many of the optimum lift distributions predicted by the theoretical methods considered here are in excellent agreement with high-fidelity solutions for various practical wing configurations and flight conditions. It follows that, in many cases, the optimum lift distributions predicted by these theoretical methods can serve as excellent benchmark solutions for higher-fidelity methods. Moreover, it is shown that theoretical aerostructural solutions provide a much more appropriate benchmark than the elliptic lift distribution.

Due to differences is design objectives, variables, and flight conditions, fully consistent comparisons between theoretical and high-fidelity aerostructural solutions for the optimum wingspan and corresponding drag are often difficult, and sometimes impossible, to make. Nevertheless, the review of these solutions in the following sections highlights important insights into the effects of viscosity, compressibility, aeroelasticity, and transonic shock on optimum aerostructural designs. Where consistent comparisons are possible, the optimum wingspan and corresponding drag from theoretical studies shows relatively good agreement with multi- and high-fidelity solutions.

In some respects, this paper can be thought of as a survey of the subset of theoretical literature concerning aerostructural optimization for minimum drag. However, in this paper, no attempt is made to present a comprehensive review of the complete body of comparable high-fidelity aerostructural literature. Instead, we have selected only a few available solutions from several multi- and high-fidelity studies [44-46,49-61] with constraints that are most comparable to those used in the theoretical studies discussed here. In the following sections, solutions are grouped into three major categories: 1) those that include constraints involving the integrated bending moment [33,37,39,44,45], 2) those with constraints involving the root bending moment [34,36,38,49-52], and 3) those that combine constraints on wing stress and deflection with operational constraints related to either wing stall [42,46,53,60] or wing loading [40-43,54-59,61].

II. Integrated Bending Moment Constraints

In 1933, Ludwig Prandtl published one of the first known studies [33] involving minimizing drag under structural constraints. In this publication [33], Prandtl presented a method for identifying the optimum lift distribution and

wingspan that minimize induced drag, including the effects of the wing weight. Prandtl's study included constraints on the gross lift and the moment of inertia of gross lift, which is derived from the integrated bending moment. To obtain an analytic solution, Prandtl assumed that the wing bending moments are solely due to the lift distribution, regardless of the weight of the wing. Prandtl also assumed that the wing bending moments $\widetilde{M}_b$ are related to the wing-structure weight W_s by a spanwise-invariant proportionality coefficient S_b, i.e.,

$$W_s = \int_0^{b/2} \frac{\widetilde{M}_b(y)}{S_b} dy \tag{2}$$

where b is the wingspan and y is the spanwise coordinate. This assumption corresponds to rectangular wings. Within the framework of these constraints and assumptions, Prandtl identified a bell-shaped lift distribution that allows a 22.5% larger wingspan and produces 11.1% less induced drag than the elliptic lift distribution with the same wing weight [33].

Prandtl's solution was revisited in 1975 by Klein and Viswanathan [39] and in 1980 by Jones and Lasinski [37]. Klein and Viswanathan noted that the wing-structure weight is not only dependent on the bending-moment distribution, but it also depends on the distribution of shear force in the wing. Thus, in addition to constraints of fixed gross lift and integrated bending moment, Klein and Viswanathan [39] imposed a constraint on the integrated shear force. Their solution results in a 16% larger wingspan and about 7% less induced drag than the elliptic lift distribution for the same wing-structure weight, or about 6% smaller wingspan and 4% more induced drag than Prandtl's solution [33]. Jones and Lasinksi [37] extended Prandtl's methodology to non-planar wings and considered the effects of winglets.

Here, we compare the solutions from these three studies with integrated bending-moment constraints to solutions from two more recent high-fidelity aerostructural optimization studies by Zhang [44] and Hoogervorst and Elham [45]. Zhang [44] sought to minimize a combination of drag and weight by optimizing the wingspan and wing twist for an aircraft wing configuration similar to that of a Boeing 737-900, subject to constraints on the maneuver stress and buckling stress. Hoogervorst and Elham [45] sought to minimize fuel weight with respect to the wingspan and wing twist at three spanwise locations for a wing based on the Airbus A320, subject to stress and fatigue constraints. A summary of the design objectives, key design variables, and key constraints for each study is included

in Table A1 of the appendix. Note that, like Prandtl [33] and Klein and Viswanathan [39], neither Zhang [44] nor Hoogervorst and Elham [45] included constraints on the wing area.

The design objectives, variables, and constraints from these two studies are much more comprehensive than those used by Prandtl [33], Klein and Viswanathan [39], and Jones and Lasinksi [37]. However, in many respects, they are comparable. For instance, Zhang [44] sought to minimize a weighted combination of induced drag D_i and weight W of the form

$$J = \beta \frac{D_i}{D_{\text{ref}}} + (1 - \beta) \frac{W}{W_{\text{ref}}} \tag{3}$$

where D_{ref} and W_{ref} are reference drag and weight values, respectively, and β is a weighting value. However, the results considered in this section place considerably more emphasis on minimizing induced drag than weight. Hoogervorst and Elham [45] sought to minimize fuel weight, which is closely related to drag through the fuel burn. Instead of using the lift distribution as a design variable, both Zhang [44] and Hoogervorst and Elham [45] used the wingspan and wing twist as design variables. Nevertheless, as evident from lifting-line theory and as shown by Phillips and Hunsaker [62], for a wing with a given planform, the lift distribution is a direct function of the wing twist distribution.

Whereas Prandtl [33], Klein and Viswanathan [39], and Jones and Lasinksi [37] imposed constraints on the integrated bending moment, Zhang [44] used constraints on the wing stress and buckling, and Hoogervorst and Elham [45] used constraints on the wing stress and fatigue. However, Phillips et al. [41] have shown that the maximum allowable stress of the wing structure can be related to the bending moments by defining the proportionality coefficient S_b in Eq. (2) in terms of the properties of the wing structure. When viewed from this perspective, the wing stress is implicit in Eq. (2), and constraints on wing stress can be thought of as analogous to constraints on the integrated bending moment. In modern aerostructural literature, there are few, if any, studies that use constraints on the integrated bending moment and/or integrated shear force alone.

The optimum cruise lift distributions identified by Prandtl [33], Klein and Viswanathan [39], Jones and Lasinksi [37], Zhang [44] (with $\beta = 0.75$), and Hoogervorst and Elham [45] are shown in Fig. 1. The elliptic lift distribution is also included for reference. From Fig. 1, we see that Zhang's solution [44] matches Prandtl's solution very well [33]. In fact, the results given in Ref. [44] show that as β increases (i.e., more emphasis is placed on drag in

the objective function), the optimum cruise lift distribution trends more toward Prandtl's solution. The solution of Hoogervorst and Elham [45] deviates slightly from Prandtl's solution, which is unsurprising, since Hoogervorst and Elham only allowed the wing to twist at the root, the tip, and one other intermediate location [45], which results in a low-resolution approximation of the optimum lift distribution. Moreover, as shown by Wroblewski and Ansell [51], the differences between the lift distributions of Hoogervorst and Elham [45] and Prandtl [33] are consistent with discrepancies between the predicted lift distribution and that measured by experiment for wings designed to produce similar lift distributions. Despite these small differences, the lift distributions from both high-fidelity solutions show excellent agreement with Prandtl's solution [33], which is remarkable, especially considering that Zhang's [44] solution is for a wing configuration similar to that of a Boeing 737-900, and Hoogervorst and Elham [45] used a wing similar to that of an Airbus A320. In fact, both high-fidelity studies appear to agree more closely with all of the theoretical aerostructural solutions shown here than with the elliptic lift distribution.

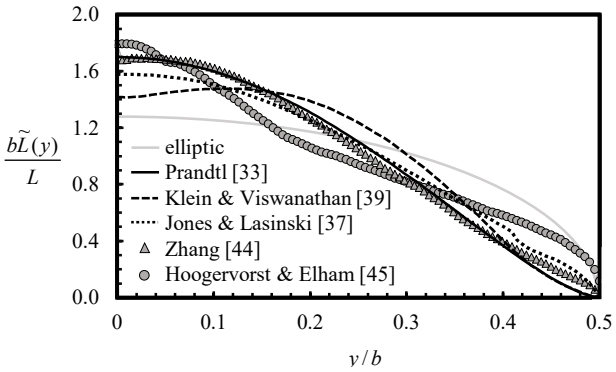

Fig. 1 Normalized optimum lift distributions from solutions with constraints related to the integrated bending moment.

Figure 2 compares the drag and wingspan from the solutions of Prandtl [33], Klein and Viswanathan [39], and Zhang [44]. For each solution, the drag and the wingspan are presented as ratios of the drag and wingspan resulting from the elliptic lift distribution on the respective study's "baseline" wing configuration. These ratios will hereafter be referred to as the "drag ratio" and the "wingspan ratio", respectively. Results from Jones and Lasinski [37] and Hoogervorst and Elham [45] were not available. Note that both Prandtl [33] and Klein and Viswanathan [39] provide solutions for the drag ratio as a function of the wingspan ratio, whereas Zhang provides results for a single, optimum configuration. The optimum solutions for Prandtl [33] and Klein and Viswanathan [39] are marked with black circles.

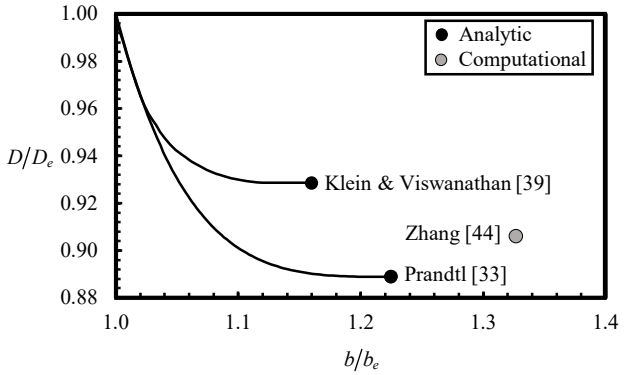

Fig. 2 Drag ratio with respect to wingspan ratio from solutions with constraints related to the integrated bending moment.

From Fig. 2, we see that whereas the drag ratio from Zhang's solution [44] falls between the drag ratios from the solutions of Prandtl [33] and Klein and Viswanathan [39], the wingspan ratio for Zhang's solution is between 10-11% higher than Prandtl's theoretical solution [33]. This difference in wingspan is consistent with solutions given by Taylor and Hunsaker [43] that include the effects of wing taper on the optimum solution. In fact, whereas Prandtl [33] and Klein and Viswanathan [39] limited their solutions to rectangular wings, Zhang used a wing configuration with a taper ratio of nearly 0.16 [44]. Using the method given by Taylor and Hunsaker [43], the optimum wingspan for a tapered wing with a taper ratio of 0.16 and Prandtl's lift distribution [33] is about 11.5% higher than the optimum wingspan for a rectangular wing with the same lift distribution, which is in excellent agreement with the wingspan difference of 10-11% shown in Fig. 2.

It is also possible that Zhang's [44] solution takes advantage of passive aeroelastic load alleviation, by which maneuver loads induce aeroelastic deflections, which result in a lift distribution that alleviates bending moments at the maneuver condition. This allows the wing to be designed with a higher wingspan than would be allowed for a wing with no passive aeroelastic load alleviation. Moreover, in the absence of constraints on the wing area, increasing the wingspan increases the aspect ratio, which tends to increase the wing flexibility and induce even more aeroelastic load alleviation. The result is a larger wingspan than that of a corresponding rigid wing. In fact, Zhang's solution [44] includes a maneuver lift distribution (not shown in Fig. 2) that features high load near the wing root and negative load near the wing tips, which results in lower bending moments at the maneuver condition than those resulting from the cruise lift distribution.

It is worth noting that the solutions of Prandtl [33] and Klein and Viswanathan [39] are both limited by the constraint that the lift distribution is fixed for all flight conditions and positive at all spanwise locations. The optimum solution for both studies lies at the limit of this second assumption, where the slope of the lift distribution at the wingtip is zero. For analytic solutions employing the methods of Prandtl [33] and Klein and Viswanathan [39], a solution having a wingspan ratio higher than the optimum shown in Fig. 2 requires negative lift at the wingtips. Under the constraints of the assumption described in Eq. (2), this would result in zero bending moment and, therefore, zero weight at some spanwise location, which is not physically valid.

III. Root Bending Moment Constraints

One of the earliest aerostructural studies including constraints on the root bending moment was presented by R. T. Jones in 1950 [34]. In his study, Jones sought to identify the lift distribution that minimizes induced drag from a family of lift distributions that produce the same root bending moment and gross lift. Under these constraints, Jones found that if the lift distribution is assumed to be all-positive, there exists a triangular-shaped lift distribution that can allow up to a 33% increase in wingspan and a reduction in induced drag of over 15% when compared to the elliptic lift distribution. However, Jones noted that nearly the same induced-drag reduction can be achieved with a 15% increase in wingspan, which, in many cases, is more practical. Thus, Jones [34] reported his "optimum" solution as having a 15% larger wingspan and producing 15% less induced drag than the elliptic lift distribution with the same root bending moment.

In the 1970's, Klein and Viswanathan [38] and DeYoung [36] obtained similar results to those found by Jones in 1950. Klein and Viswanathan [38] modified Prandtl's 1933 method [33] by replacing Prandtl's constraint on the moment of inertia of gross lift (integrated bending moment) with a constraint on the root bending moment. They found that the optimum lift distribution corresponds to a 33.3% increase in wingspan and a 15.6% reduction in induced drag over the elliptic lift distribution. DeYoung [36] obtained the same result from a more general method that allows for unconventional wing configurations by imposing a constraint on the bending moment at a prescribed location on the wing. Like the theoretical studies in the previous section, the studies of Jones [34], Klein and Viswanathan [38], and DeYoung [36] include the assumption that the bending moments are only due to the lift distribution. Moreover, by

using the root bending moment as a surrogate for wing weight and constraining the root bending moment to a fixed value, each author implicitly assumes that the wing weight is constant.

The optimum solutions from the studies of Jones [34], Klein and Viswanathan [38], and DeYoung [36] each include a considerably larger wingspan than that resulting from the elliptic lift distribution with the same root bending moment. Because no area constraints are included in any of these studies, the wing areas corresponding to the optimum solutions are also large. Since more wing area typically results in higher viscous drag, viscous effects can significantly reduce the optimality of these solutions. In 2009, Verstraetan and Slingerland [50] incorporated viscous effects and used a computational method to identify optimum solutions for both planar and nonplanar wings with fixed lift and root bending moment. For a planar wing, the solution of Verstraetan and Slingerland [50] allows a wingspan increase of 22% and a drag reduction of 8% over the elliptic lift distribution. Later, Ranjan [49] and Wroblewski and Ansell [51] obtained similar results using a similar method. However, experimental data from Wroblewski and Ansell [51] deviates slightly from the predicted optimum solution.

There are very few high-fidelity aerostructural optimization studies that incorporate root-bending-moment constraints. However, in 2014, Lyu and Martins [52] included a constraint on the root bending moment in a series of high-fidelity optimization case studies aimed at minimizing the drag coefficient at cruise on a swept-wing blended-wing-body aircraft. Lyu and Martins [52] added the root-bending-moment constraint only as a limiter within an aerodynamic optimization framework. The result was a marginal increase in the wingspan and a small reduction in drag. A summary of the design objectives and key design variables and constraints for this and each of the other studies considered in this section is given in Table A2 in the appendix.

Figure 3 shows the normalized lift distributions from the solutions of Jones [34], Klein and Viswanathan [38], DeYoung [36], Verstraetan and Slingerland [50], and Lyu and Martins [52]. The optimum lift distributions predicted by Ranjan [49] and Wroblewski and Ansell [51] for minimum inviscid drag and total drag are indistinguishable from those given by Klein and Viswanathan [38] and Verstraetan and Slingerland [50], respectively, and are therefore not shown. From Fig. 3, we see that the lift distribution from the high-fidelity solution of Lyu and Martins [52] is most similar to the lift distribution given by Jones [34].

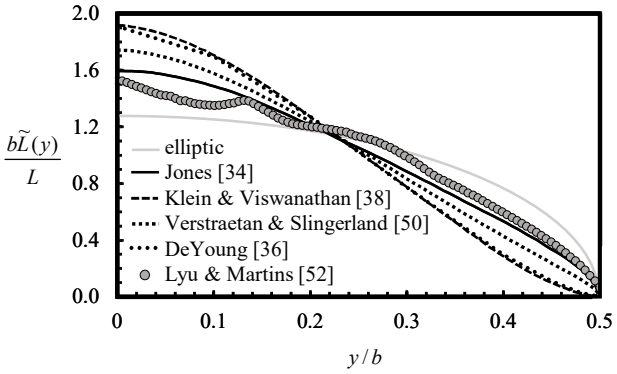

Fig. 3 Normalized optimum lift distributions from solutions with constraints related to the root bending moment.

Figure 4 shows the drag and wingspan ratios for each of the solutions discussed in this section. The results in Fig. 4 include two groups: analytic solutions that consider only induced drag [34, 36, 38], which are shown in black, and computational solutions that include viscous effects [49-51], which are shown in gray. The experimental results from Wroblewski and Ansell [51] are for wing designs based on the optimum solutions of Ranjan [49] and Klein and Viswanathan [38]. Notice that the high-fidelity solution given by Lyu and Martins [52] falls very near unity for both the wingspan ratio and drag ratio. This is somewhat surprising, since Fig. 3 shows that the optimum lift distribution from this solution is similar to that given by Jones [34]. Nevertheless, Lyu and Martins [52] note that any additional increase in wingspan is limited by the root bending moment and by the increase in viscous drag due to additional wing surface area.

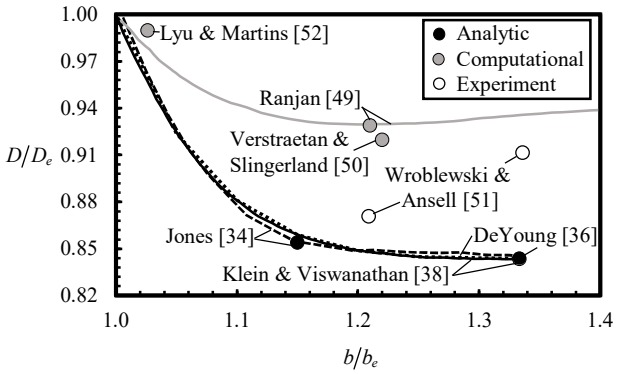

Fig. 4 Drag ratio with respect to wingspan ratio from solutions with constraints related to the root bending moment.

The difference between the results of Ranjan [49] and Verstraetan and Slingerland [50] and those of Jones [34], Klein and Viswanathan [38], and DeYoung [36] highlight the importance of viscous drag on the optimum solution. In

low-speed cruise, viscous drag makes up about half of the total drag. Because of this, any reduction in induced drag shown in Fig. 4 corresponds to a much smaller reduction in total drag. In fact, if viscous drag remains relatively constant, we should expect that the induced drag reductions of around 15% reported by Jones [34], Klein and Viswanathan [38], and DeYoung [36] translate to only about 7 or 8% total drag reduction, which agrees very well with the computational results of Ranjan [49] and Verstraetan and Slingerland [50]. Moreover, as noted by Jones [34] viscous drag effectively limits the optimum wingspan, since large increases in wingspan correspond to more wetted area and higher viscous drag, which offsets the induced-drag benefits obtained by increasing the wingspan. Thus, the results of Ranjan [49] and Verstraetan and Slingerland [50] have lower wingspans than the inviscid results of Klein and Viswanathan [38] and DeYoung [36]. When viscous effects are considered, these two viscous solutions [49,50] and Jones' "optimum" solution, which produces nearly minimum induced drag with a much smaller wingspan and wing area than the true minimum-induced-drag solution, are likely to have less total drag than those given by Klein and Viswanathan [38] and DeYoung [36].

Like the solutions of Prandtl [33] and Klein and Viswanathan [39] shown in the previous section, the solutions of Jones [34], Klein and Viswanathan [38], and DeYoung [36] are limited to all-positive lift distributions. In each case, the optimum lift distribution again lies at the limit of this assumption, where the lift distribution has zero slope at the wingtip. However, the result of Ranjan [49] shows that when viscous effects are considered, the optimum wingspan falls well below the maximum allowed under the all-positive lift-distribution constraint.

IV. Stress and Deflection Limits with Operational Constraints

In each of the studies shown in the previous two sections, the wingspan is allowed to vary without any constraint on the wing area. However, Iglesias and Mason [31] point out that under this constraint, changing the wingspan changes the wing area, which results in a comparison between wings with fundamentally different operational performance characteristics. Since aircraft are typically designed to meet at least one specified performance parameter, it is unhelpful to compare any "optimized" wing to a baseline configuration if the "optimum" wing does not have similar operational performance characteristics as the baseline wing. In order to ensure a fair comparison, Phillips et al. [41,42] suggested that the wing design should be constrained so that either the wing loading, which affects several key airspeed requirements, or stall speed, which is critical for takeoff and landing performance, is fixed. Therefore, in

this section, we will consider several studies that combine wing stress and deflection constraints with constraints related to either wing stall or the wing loading.

Phillips et al. [41,42] give the largest set of theoretical solutions in this category. Revisiting Prandtl's 1933 assumption that the wing-structure weight is proportional to the bending moments, Phillips et al. [41,42] used simple beam theory to define the proportionality coefficient S_b in terms of the beam geometric and material properties, i.e., [41],

$$W_s = \int_0^{b/2} \frac{\left|\widetilde{M}_b(y)\right|}{S_b(y)} dy; \quad S_b(y) \equiv \frac{C_\sigma (t_{\max}/c) c(y) \sigma_{\max}}{\gamma}, \quad C_\sigma \equiv \frac{2I(h/t_{\max})}{Ah^2} \tag{4}$$

where $t_{\max}/c$ is the wing thickness-to-chord ratio, c is the wing chord, $\sigma_{\max}$ is the maximum allowable stress, γ is the specific weight of the wing-structure material, and I, A, and h are the second moment of inertia, area, and height of the wing structure, respectively. Note that Eq. (4) is analogous to Eq. (2) but includes a limit on the maximum allowable bending stress. Thus, Eq. (4) describes the wing-structure weight for the stress-limited design. Phillips et al. [41] also included deflection constraints by relating the maximum allowable deflection to the maximum allowable stress to give [41]

$$W_s = \int_0^{b/2} \frac{\left|\widetilde{M}_b(y)\right|}{S_b(y)} dy; \quad S_b(y) \equiv \frac{C_\delta E (t_{\max}/c)^2 c(y)^2 \delta_{\max}}{\gamma}, \quad C_\delta \equiv \frac{8I(h/t_{\max})^2}{Ah^2} \tag{5}$$

where E is the modulus of elasticity of the wing-structure material, and $\delta_{\max}$ is the maximum allowable deflection. Thus, Eq. (5) describes the wing-structure weight for the deflection-limited design.

Whereas Prandtl [33] assumed that the wing bending moments are a function of the lift distribution alone, Phillips et al. [41,42] assumed that the bending moments are related to the lift distribution and wing weight distribution according to the relation [41]

$$\widetilde{M}_b(y) = \int_{z'=z}^{b/2} [\widetilde{L}(y') - n_a \widetilde{W}_n(y') - n_a \widetilde{W}_s(y')](y'-y) dy', \quad \text{for } y \geq 0 \tag{6}$$

where n_a is the load factor at the design limit, $\widetilde{W}_n(y)$ is the weight of all non-structural components in the wing, and $\widetilde{L}(y)$ is the section lift distribution. At all points, the wing structure must be designed to support the bending moments encountered during a high-load maneuver and during a negative-load maneuver, such as a hard landing. To obtain analytic results, Phillips et al. [41,42] assumed that the lift distribution is fixed for all flight phases. For each of the

four cases considered here (stress-limited design with fixed stall speed, deflection-limited design with fixed stall speed, stress-limited design with fixed wing loading, and deflection-limited design with fixed wing loading), Phillips et al. [41,42] found that the optimum lift distribution depends only on the design constraints and is independent of all other design parameters.

A. Stall-Related Constraints

For most aircraft, the takeoff and landing performance are heavily influenced by the stall speed V_{stall}. For example, FAR regulations dictate that the takeoff speed must be at least 10% higher than the stall speed and that reference landing speed must be 30% higher than the stall speed. Because of this, the stall speed can be constrained to ensure that any optimal wing design maintains similar takeoff and landing performance to the baseline design. Phillips et al. [41,42] defined the stall speed as the speed at which stall begins at any section of the wing. This happens when the local lift coefficient exceeds the maximum lift coefficient $\widetilde{C}_{L_{\max}}$ of the airfoil section. For a rectangular wing with chord c and lift distribution $\widetilde{L}(y)$, this occurs when

$$\frac{\widetilde{L}(y)_{\max}}{\frac{1}{2}\rho V_{\text{stall}}^2 c} = \widetilde{C}_{L_{\max}} \tag{7}$$

Equation (7) shows that for a given lift distribution and freestream density, the stall speed and maximum lift coefficient are related. If $\widetilde{C}_{L_{\max}}$ is fixed, then the chord must change to ensure that the local lift coefficient does not exceed $\widetilde{C}_{L_{\max}}$, which alters the wing area.

1. Stress-Limited Design

Under the constraint of fixed stall speed, Phillips et al. [42] found that the optimum lift distribution for the stress-limited design is the same as that found by Prandtl in 1933 [33] for a rectangular wing with fixed weight and moment of inertia of gross weight. This lift distribution is shown in Fig. 5, alongside the optimum lift distribution from a high-fidelity study by van den Kieboom and Elham [53] aimed at minimizing fuel burn for a Fokker 100 class regional jet aircraft wing in low-speed flight with fixed maximum takeoff weight (MTOW). In this study, the lift distribution is controlled by a small number of discrete high-lift flaps. The flap deflection, flap shape, wingspan, and wing shape are all included as design variables, and the wing is subject to constraints on wing stress and takeoff and landing distance.

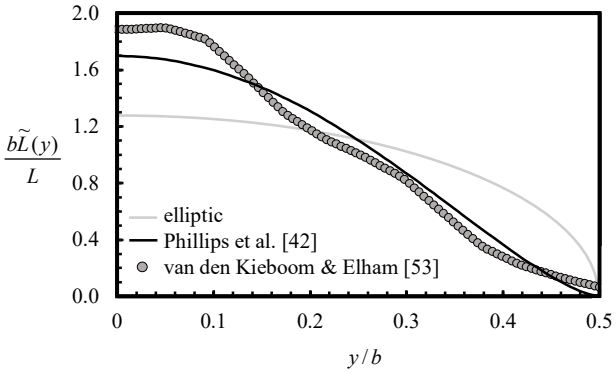

Fig. 5 Normalized optimum lift distributions from solutions with constraints related to the wing stress and the stall speed.

Although van den Kieboom and Elham [53] did not explicitly enforce constraints on the stall speed, Phillips [63] has shown that the no-wind takeoff distance $s_{\mathrm{g,TO}}$ for an aircraft with a takeoff speed of $1.1V_{\mathrm{stall}}$ can be approximated as [63]

$$s_{g,TO} \cong \frac{1.21W^2}{\rho g S_w C_{L_{\max}} (T - D - F_r)_{0.77V_{\mathrm{stall}}}} + 1.1 t_r V_{\mathrm{stall}} \tag{8}$$

where S_w is the wing area, t_r is the rotation time, and the thrust $T = T(V)$, the drag $D = D(V)$, and the rolling friction $F_r = F_r(V)$ are evaluated at 77% of the stall speed. The landing distance $s_{\mathrm{g},L}$ for an aircraft with a landing speed of $1.3V_{\mathrm{stall}}$ can be approximated as [63]

$$s_{g,L} = \frac{W/S_w}{\rho g (C_D - \mu_r C_L)} \ln\left[1 + \frac{1.69\rho V_{\mathrm{stall}}^2}{2W/S_w}\left(\frac{C_D}{\mu_r} - C_L\right)\right] + 1.30 t_f V_{\mathrm{stall}} \tag{9}$$

where t_f is the brake-engagement reaction time, μ_r is the coefficient of rolling friction, and C_L and C_D are constant. Equations (8) and (9) show that for a wing with fixed MTOW, S_w, and $\widetilde{C}_{L_{\max}}$ on a surface with known μ_r, constraints on takeoff and landing distance are a function of the stall speed. Thus, van den Kieboom and Elham's [53] constraints on the takeoff and landing distance are closely related to the stall speed. A summary of the key design variables and constraints for the studies of Phillips et al. [42] and van den Kieboom and Elham [53] are given in Table A4 in the appendix.

Figure 5 shows that the lift distributions of Phillips et al. [42] and van den Kieboom and Elham [53] are in general agreement but exhibit some differences. As was the case with Hoogervorst and Elham [45], these differences are likely due to the relatively low number of flaps used by van den Kieboom and Elham [53] to control the lift distribution,

which results in a low-resolution approximation of the optimum lift distribution. Figure 6 shows that the wingspan ratio and corresponding drag ratio from van den Kieboom [53] agree relatively well with those predicted by Phillips et al. [42].

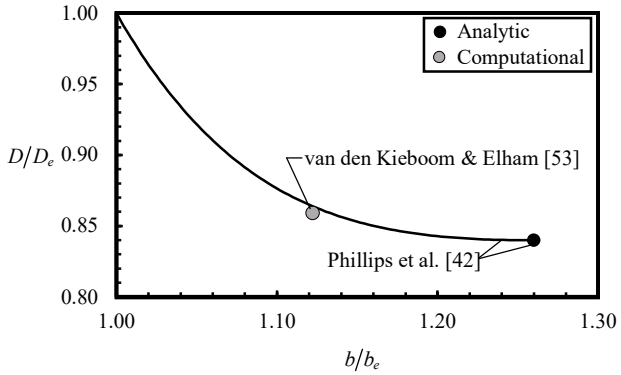

Fig. 6 Drag ratio with respect to wingspan ratio from solutions with constraints related to the wing stress and the stall speed.

2. Deflection-Limited Design

In addition to stress constraints, Phillips et al. [41,42] also considered constraints on the static wing deflection. Although static wing deflection constraints are seldom, if ever, enforced in practice, wing deflection can have significant aerodynamic effects, especially for highly flexible wings. Although flexible wings often benefit from some passive aeroelastic maneuver load alleviation, excessive wing deflection can negatively impact cruise performance. Conceptually, there is some limit on flexibility at which negative effects during cruise outweigh passive load alleviation during a maneuver. This limit can be thought of as a "soft" deflection limit. Because wings with high aspect ratios often have greater flexibility, this "soft" limit on wing deflection can also serve as a limit on the aspect ratio. Thus, although Phillips et al. [41,42] did not account for the aerodynamic effects of static wing deflections, their "hard" deflection limit acts as a surrogate for the natural aerostructural efficiency limit associated with high-aspect-ratio designs.

The optimum lift distribution found by Phillips et al. [42] for the deflection-limited design of a wing with fixed stall speed is shown in Fig. 7, alongside four additional lift distributions from high-fidelity solutions found by Jansen et al. [46] for a flexible tapered wing with wingtip devices and three lift distributions from a high-fidelity study by Mader et al. [60] for the flexible D8 wing in transonic flight with cruise Mach numbers of 0.72, 0.78, and 0.82. In

their study, Jansen et al. [46] sought to minimize induced and total drag on wings with winglets and raked wingtips using design variables including the wingspan, jig twist, sweep angle, and dihedral distribution, with constraints on lift, maneuver stress, and wing stall. The results labeled *a, b, c,* and *d* in Fig. 7 correspond to solutions for minimum total drag with raked wingtips (*a*), minimum total drag with winglets (*b*), minimum induced drag with winglets (*c*), and minimum induced drag with raked wingtips (*d*). Mader et al. [60] sought to minimize fuel burn using wingspan, twist, airfoil shape, sweep angle, and other design variables, subject to constraints on the wing stress, pitching moment, and flow separation.

It is important to note that in place of a constraint on the stall speed, Jansen et al. [46] placed a constraint on the maximum section lift coefficient $\widetilde{C}_{L_{\max}}$, and Mader et al. [61] included a constraint on flow separation to preclude stall due to buffet. Although these constraints differ from the fixed-stall-speed constraint used by Phillips et al. [42], the stall speed and $\widetilde{C}_{L_{\max}}$ are related through Eq. (7), and since stall is a result of flow separation, the stall speed and $\widetilde{C}_{L_{\max}}$ can be thought of as surrogate indicators of flow separation. Thus, the constraints on flow separation are also closely related to the stall speed and $\widetilde{C}_{L_{\max}}$.

Figure 7 shows that the optimum lift distribution of Phillips et al. [42] falls well within the range of solutions given by Jansen et al. [46] and shows good agreement with the results given by Mader et al. [61], with the closest agreement at $M = 0.82$. The reason for this may be that at $M = 0.82$, the flow-separation constraint is most active. In fact, the results from Mader et al. [61] show little to no flow separation at $M = 0.72$ and $M = 0.78$, but indicate small regions of flow separation at $M = 0.82$, which suggests that at this Mach number, the optimum design may be approaching the constraining flow-separation limit.

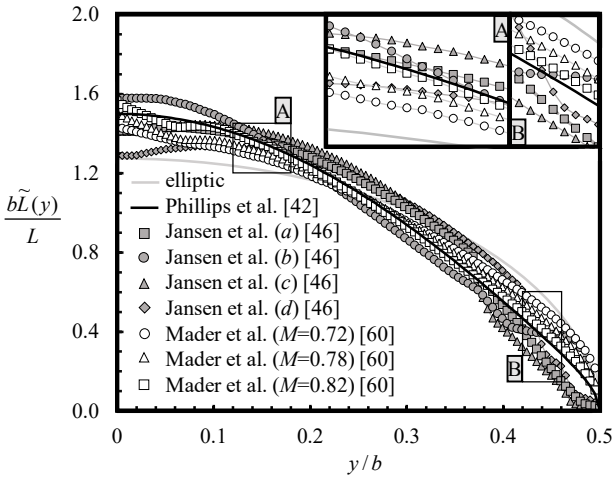

Fig. 7 Normalized optimum lift distributions from solutions with constraints related to the wing deflection and the stall speed.

The drag ratio and wingspan ratio for the solutions of Phillips et al. [42] and Jansen et al. [46] are shown in Fig. 8. Results from Mader et al. [60] were not available. Although the wingspan ratios given by Jansen et al. [46] are generally higher than that given by Phillips et al. [42], we see that the solutions of Jansen et al. [46] follow the general trend of the solution of Phillips et al. [42] reasonably well. Note that because Jansen et al. [46] did not include the vertical portion of the winglet in the wingspan measurement, the solutions for wings with raked wingtips (*a* and *d*) have significantly higher wingspan ratios than the solutions for wings with winglets (*b* and *c*). As was the case with Zhang [44] and Prandtl [33], the difference in wingspan between the solutions of Jansen et al. [46] and Phillips et al. [42] is likely due, at least in part, to both aeroelastic load alleviation and the effects of wing taper. In fact, whereas Phillips et al. [42] limited their solutions to rectangular wings, each of the solutions from Jansen et al. [46] includes a wing with a small taper ratio. As shown by Taylor and Hunsaker [43], taper ratios below 0.2 can result in up to a 10-15% larger wingspan ratio than is possible with a rectangular wing. Thus, the differences in wingspan ratio between the solutions of Jansen et al. [46] and the solution of Phillips et al. [42] are not surprising. Moreover, as expected, the minimum-induced-drag solutions from Jansen et al. [46] (*c* and *d*) have lower drag ratios, and agree with the solution of Phillips et al. [42] better, than the minimum-total-drag solutions (*a* and *b*), which also include viscous and compressibility effects.

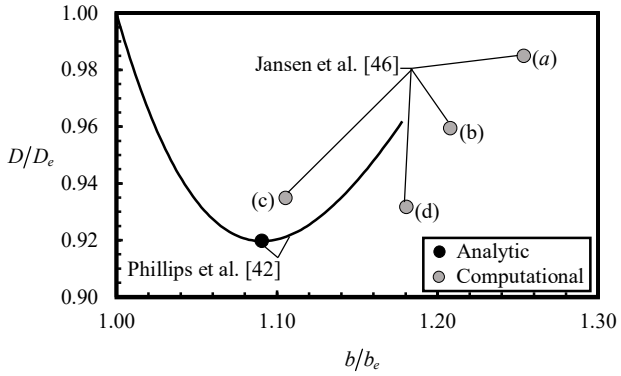

Fig. 8 Drag ratio with respect to wingspan ratio from solutions with constraints related to the wing deflection and the stall speed.

B. Wing-Loading Constraints

The wing loading W/S_W is an important parameter that affects several aircraft performance metrics. For example, Eqs. (8) and (9) show that the wing loading affects the takeoff and landing performance. Phillips [63] has shown that the wing loading also affects several key performance airspeeds. Therefore, fixing the wing area ensures that any optimum wing design has similar performance to the baseline wing design. In order to maintain fixed wing loading with no constraint on the wing weight, the wing area must be constrained such that as the weight changes, the wing area changes to maintain the wing loading. This is the approach taken by Phillips et al. [42] and Taylor and Hunsaker [43]. However, if the weight is fixed, then the wing area must also be fixed, as was done by Phillips et al. [41], Stewart and Hunsaker [61], Löbert [40], McGeer [54], Piperni et al. [55], Liem et al. [56] and Elham and van Tooren [58]. Here, we will also consider results from studies by Kenway et al. [59] and Ning and Kroo [57], in which the wing area is fixed with no constraint on the weight. In general, this allows for changes in the wing loading. However, in Ref. [59], the wing loading changes by only 1.7%. In Ref. [57], the weight is not given, but we assume that changes in wing loading are similarly small.

1. Stress-Limited Design

Key results from several studies with constraints related to the wing stress and wing loading are shown in Figs. 9 and 10. Figure 9 shows the optimum cruise lift distribution from each study, and Fig. 10 shows the optimum wingspan and drag ratios. Results shown in Fig. 9 include the theoretical studies of Phillips et al. [41,42], Taylor and Hunsaker [43] (with $R_T = 0$), and Löbert [40]; the multi-fidelity results of Stewart and Hunsaker [61] (with geometric and aerodynamic twist) and McGeer [54]; and the high-fidelity studies of Piperni et al. [55], Ning and Kroo [57], Liem et al. [56], and Elham and van Tooren [58]. A summary of the optimization objectives, key design variables, and key

design constraints for each of these studies is given in Table A5 in the appendix. Note that because Piperni et al. [55], Ning and Kroo [57], and Elham and van Tooren [58] do not give data for the drag and wingspan ratios, their solutions are not included in Fig. 10.

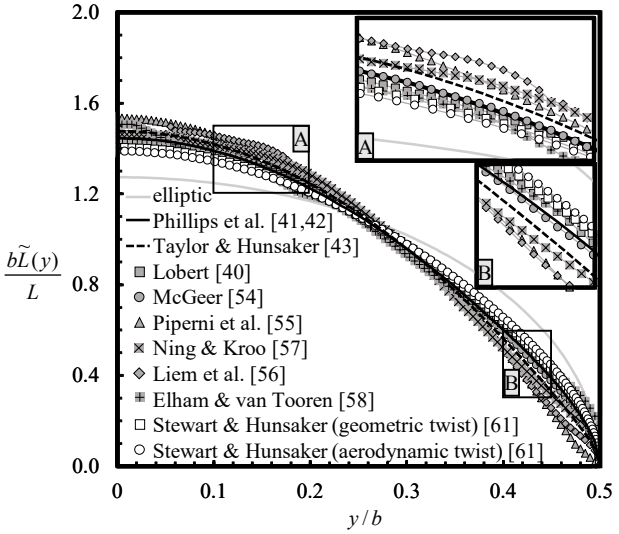

Fig. 9 Normalized optimum lift distributions from solutions with constraints related to the wing stress and the wing loading.

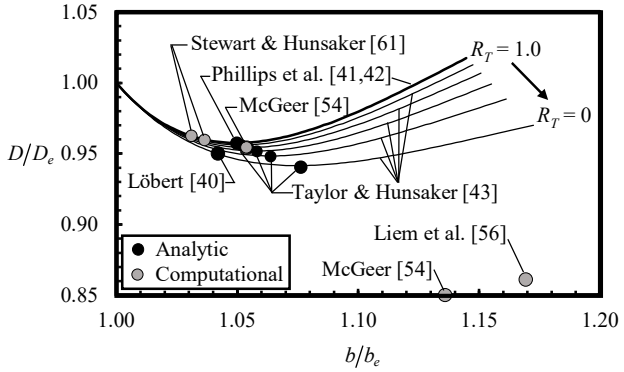

Fig. 10 Drag ratio with respect to wingspan ratio from solutions with constraints related to the wing stress and the wing loading.

The most striking observation from Fig. 9 is the high level of agreement between all of the cruise lift distributions shown, despite significant differences in the design objectives, variables, and assumptions used in each study. Phillips et. al [41,42] used only the wingspan and lift distribution as design variables to minimize induced drag on a planar, unswept rectangular wing. Taylor and Hunsaker [43] extended the work of Phillips et al. [41,42] to tapered wings. Stewart and Hunsaker [61] considered the effects of parasitic drag on the results given by Phillips et al. [41,42] when the lift distribution is achieved using either geometric or aerodynamic twist alone. The approaches of Löbert [40] and

McGeer [54] are similar to those of Phillips et al. [41,42] and Taylor and Hunsaker [43], but both considered swept wings, and McGeer [54] allowed the airfoil thickness to change, while imposing constraints on the parasitic drag. In the high-fidelity study by Ning and Kroo [57], the cruise and maneuver twist distributions are treated as separate design variables and are optimized to minimize total drag on a trapezoidal wing typical of a commercial transport. Piperni et al. [55] sought to minimize the cash operating cost on the wing of a large transonic business jet, including the effects of wing flexibility. Liem et al. [56] and Elham and van Tooren [58] sought to minimize the fuel burn on the Common Research Model wing and a wing similar to the Airbus A320, respectively, both including aeroelastic and transonic effects. The agreement of the results in Fig. 9 suggests that the optimum cruise lift distribution for a wing with stress and wing-loading constraints is relatively consistent over a wide range of aircraft configurations and flight conditions and is well-approximated by the theoretical solutions of Phillips et al. [41,42], Taylor and Hunsaker [43], and Löbert [40].

Figure 10 shows the optimum drag ratios and wingspan ratios for solutions given by Phillips et al. [41,42], Taylor and Hunsaker [43], Stewart and Hunsaker [61], Löbert [40], McGeer [54] and Liem et al. [56]. Note that the wingspan ratios from the solutions of Stewart and Hunsaker [61] are slightly smaller, and the drag ratios are slightly higher, than the optimum solutions given by Phillips et al. [41,42], Taylor and Hunsaker [43], and Löbert [40]. Although Stewart and Hunsaker [61] used very nearly the same constraints as Phillips et al. [41,42] and Taylor and Hunsaker [43], the solutions of Stewart and Hunsaker [61] are for minimum total drag, whereas the results of Phillips et al. [41,42], Taylor and Hunsaker [43], and Löbert [40] are for minimum induced drag. Since in each of these cases, the wing-structure weight is constant, the wing area must also be constant, and changes in parasitic drag are primarily a result of changes in geometric or aerodynamic twist. Figure 9 shows that the lift distributions from Phillips et al. [41,42] and Taylor and Hunsaker [43], which minimize induced drag, feature higher lift at the wing root and lower lift at outboard portions of the wing than the elliptic lift distribution. However, on a rectangular wing, these lift distributions require more twist, and therefore, produce more parasitic drag than lift distributions that are more nearly elliptic. Therefore, when minimizing total drag on subsonic wings with fixed wing area, there is a tradeoff between induced and parasitic drag resulting from the relationship between the lift distribution, wing twist, and drag. The result of this tradeoff is an optimum lift distribution that is slightly more elliptic, and requires less twist, than the optimum lift distribution for minimum induced drag, as shown in Fig. 9. If the wing-structure weight is fixed, then the corresponding wingspan

ratio is slightly lower, and the drag ratio is slightly higher, than the minimum-induced drag solution. This is reflected in the differences between the solutions of Stewart and Hunsaker [61] and those of Phillips et al. [41,42], Taylor and Hunsaker [43], and Löbert [40] in Fig. 10.

It is also important to note that two solutions from McGeer [54] are included in Fig. 10. Both are solutions for the design of a light, low-speed wing. The only difference between these two solutions is that the solution at the bottom of Fig. 10 includes the airfoil thickness as a design variable, while the solution near those of Phillips et al. [41,42], Taylor and Hunsaker [43], and Löbert [40] only includes the wingspan and lift distribution as design variables. Within the constraints of McGeer's study [54], the allowable height of the wing structure inside the airfoil section increases as the airfoil thickness increases, which reduces the amount of structure needed to support a given distribution of wing bending moments. Since McGeer's solution is for a low-speed wing, the airfoil thickness is not constrained by transonic effects, which tend to favor thin airfoils that reduce transonic shock. Thus, when the thickness is included as a design variable, as is the case with McGeer's solution [54], we expect the solution to favor a thick airfoil that allows for a more efficient wing-structure design and results in a higher wingspan and lower drag than solutions with prescribed thickness, such as those in Refs. [40,41,42,54].

In the case of Liem et al. [56], the relatively high wingspan ratio and low drag ratio shown in Fig. 10 are likely due to several effects, including passive aeroelastic load alleviation, as described in Section II, and wave-drag reduction. Whereas all other solutions in Fig. 10 are for low-speed flight, the solution given by Liem et al. [56] is for flight in the transonic regime, where wave drag constitutes a significant portion of total drag. Wave drag can be reduced by changing wing sweep and by tailoring the airfoil cross sections to delay shock. In fact, in their study, Liem et al. [56] include the sweep angle and the airfoil shapes as design variables and show that the wave drag is the largest contributor to the drag reduction achieved by their optimum solution. Thus, it is not surprising that the solution of Liem et al. [56] has a much lower drag ratio than those corresponding to most low-speed solutions.

2. Deflection-Limited Design

Phillips et al. [41,42] also presented a solution for the deflection-limited design of a wing with fixed wing loading. Here, we compare this solution to the minimum-drag solution presented by McGeer [54] for a light, high-speed elastic wing with fixed wing-structure weight and fixed wing area and the minimum-fuel-burn solution presented by Kenway et al. [59] for the flexible undeflected Common Research Model wing in transonic flight. A summary of the

optimization setup for each of these studies is given in Table A6 in the appendix. The optimum lift distribution from each solution is shown in Fig. 11, and the corresponding drag ratios and wingspan ratios are shown in Fig. 12.

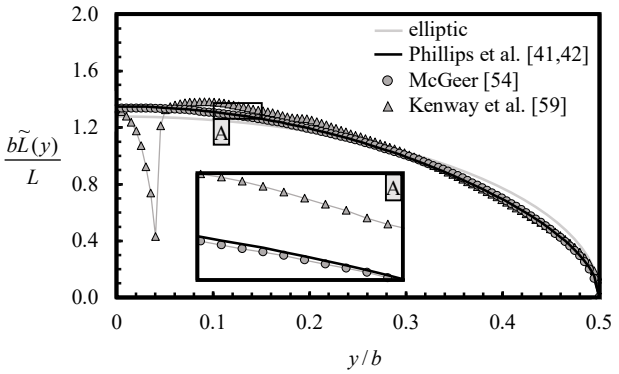

Fig. 11 Normalized optimum lift distributions from solutions with constraints related to the wing deflection and the wing loading.

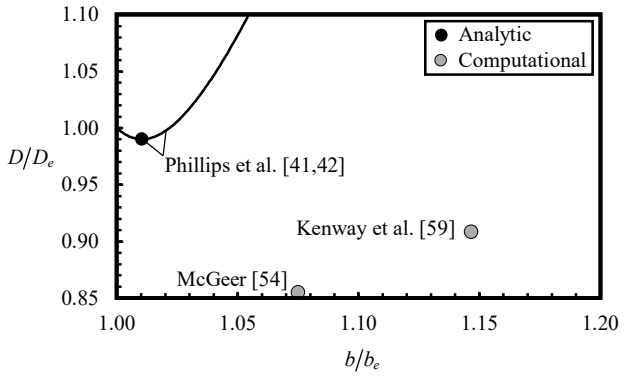

Fig. 12 Drag ratio with respect to wingspan ratio for solutions with constraints related to the wing deflection and the wing loading.

From Fig. 11, we see that, as was the case for solutions with stress and wing-loading constraints, the optimum lift distribution from solutions with deflection and wing-loading constraints show remarkable consistency, especially considering the range of configurations and flight conditions represented by these three studies. However, as expected, the wingspan and drag ratios of McGeer [54] and Kenway et al. [59] shown in Fig. 12 are significantly different from those given by Phillips et al. [41,42]. Again, in the case of McGeer [54], this is likely due to thickness effects, and in the case of Kenway et al. [59], this is likely due to passive aeroelastic load alleviation and wave drag reduction achieved by changing the sweep angle and airfoil shapes.

V. Conclusions

As aerostructural research trends more toward computational methods, theoretical aerostructural solutions are often neglected and are sometimes forgotten. However, as evidenced by the aerodynamically-optimum elliptic lift distribution, solutions based on theory can sometimes have value well beyond the assumptions of the original theory. Because of this, in this paper, we have sought to address two foundational questions regarding theoretical solutions: 1) How well do theoretical aerostructural solutions apply to practical aircraft configurations? and 2) Can these solutions be used as a benchmark for higher fidelity methods? By comparing several theoretical solutions to high-fidelity solutions with comparable design constraints, it has been shown that whereas equal comparisons between solutions for the optimum wingspan and induced drag are often difficult to obtain, theoretical solutions for optimum lift distributions consistently show good agreement with results from high-fidelity studies for a wide variety of design constraints and wing configurations. It follows that theoretical optimum lift distributions from aerostructural theories can, in many cases, serve as an appropriate benchmark for higher fidelity solutions.

For appropriate comparison, the results in this paper are divided into categories based on the design constraints. Section II compares solutions from studies with constraints related to the integrated bending moment, with no other constraint on wing area. Section III compares solutions from studies with constraints on the root bending moment. Section IV compares solutions combining constraints related to wing stress or wing deflection with constraints on either wing stall or the wing loading. The results are summarized in Figs. 1-12.

The optimum lift distributions for each of these categories are shown in Figs. 1, 3, 5, 7, 9, and 11. Each of these figures show excellent agreement between the theoretical optimum lift distributions and lift distributions from high-fidelity studies. Of the studies considered here, the best agreement is shown in Figs. 9 and 11, which compare solutions for wings with constraints related to the wing loading, combined with constraints related to the wing stress and wing deflection, respectively. In these figures, the theoretical solution matches the high-fidelity solutions very well, suggesting that for this case, the optimum lift distribution is driven primarily by the design constraints. Moreover, it has been shown that the theoretical aerostructural lift distributions shown here are in much better agreement with high-fidelity solutions, and therefore, provide a much more appropriate benchmark, than the elliptic lift distribution.

Solutions for the optimum wingspan and corresponding drag for the studies in each design-constraint category are shown in Figs. 2, 4, 6, 8, 10, and 12. Because of variations in the design objectives, variables and assumptions, a true

comparison of drag and wingspan values often cannot be obtained. However, by reviewing these solutions, it has been shown that the wingspan and drag values from each of these studies exhibit reasonable trends, and where equal comparisons are possible, the solutions from theoretical and computational studies are in good agreement.

It should be remembered that the studies considered in this paper do not represent an exhaustive review of the aerostructural literature. Instead, this paper only focuses on the specific subset of theoretical aerostructural studies concerned with minimizing drag with respect to the wingspan and the lift distribution. The multi- and high-fidelity studies shown here were selected based on their design constraints to provide as appropriate a comparison as possible to the theoretical results. It should also be remembered that the results and discussion in this paper do not provide an explanation of all of the physical mechanisms that contribute to the solutions shown here. Nevertheless, the results shown in this paper highlight the value of theoretical aerostructural solutions for gaining insights into the aerodynamic and structural coupling involved in aerostructural design and optimization and for benchmarking higher fidelity methods.

Appendix

The following tables give a summary of the key design objectives, design variables, and design constraints for each of the aerostructural studies discussed in this paper. Table A1 includes studies with constraints related to the wing integrated bending moment. Table A2 shows studies with constraints related to the wing root bending moment. Tables A3 and A4 are for studies combining constraints on the wing stress and deflection with constraints related to wing stall. Tables A5 and A6 are for studies combining constraints on the wing stress and deflection with constraints related to the wing loading. For each table, the primary constraints or assumptions that relate to these categories are typeset in bold, along with key design variables related to the wingspan and lift distribution. It should be remembered that these tables are intended for high-level reference and comparison only. In many cases, the design variables and constraints shown here do not represent an exhaustive list of all design variables and constraints considered in the respective study.

Table A1 Optimization summary and key constraints for studies including constraints related to the integrated bending moment.

	study type	*configuration*	*objective*	*key design variables*	*key constraints*
Prandtl [33]	analytic	planar, unswept rectangular wing	minimum induced drag	**wingspan** **lift distribution**	fixed gross weight **fixed moment of inertia of weight** fixed chord fixed *t*/*c*
Klein & Viswanathan [39]	analytic	planar, unswept wing	minimum induced drag	**wingspan** **lift distribution**	fixed wing-structure weight fixed lift **max integrated bending moment** max integrated shear force
Jones & Lasinski [37]	analytic	unswept wing with winglets	minimum induced drag	**wingspan** **lift distribution**	**max integrated bending moment** fixed weight
Zhang [44]	high fidelity	Boeing 737 (similar)	minimum linear combination, induced drag & weight	**wingspan** **twist distribution** airfoil shape angle of attack structure thickness	**max maneuver stress** fixed net weight fixed Mach number fixed altitude
Hoogervorst & Elham [45]	high fidelity	Airbus A320 (similar)	minimum fuel weight	**wingspan** **break, tip twist** airfoil shape angle of attack root chord taper ratio sweep angle structure thicknesses takeoff weight	steady level lift coefficient **max stress, 2.5 g pull up** **max stress, -1.0 g push over** max fatigue stress, 1.3 g gust **max stress, 1.0 g roll** min aileron effectiveness

Table A2 Optimization summary and key constraints for studies including constraints related to the root bending moment.

	study type	*configuration*	*objective*	*key design variables*	*key constraints*
Jones [34]	analytic	planar, unswept wing	minimum induced drag	**wingspan** **lift distribution**	fixed lift **fixed root bending moment**
Klein & Viswanathan [38]	analytic	planar, unswept wing	minimize induced drag	**wingspan** **lift distribution**	fixed lift **fixed root bending moment**
DeYoung [36]	analytic	planar, unswept wing	minimum induced drag	**wingspan** **lift distribution**	fixed lift **fixed bending moment, given location**
Verstraetan & Slingerland [50]	multi fidelity	unswept wing with winglets	minimum drag	**wingspan** **lift distribution** winglet height winglet length	fixed lift **fixed root bending moment** fixed wing area
Ranjan [49]	multi fidelity	planar, unswept wing	minimum drag	**wingspan** **twist distribution** chord	fixed lift **fixed root bending moment, maneuver** fixed wing area fixed Reynolds number fixed airfoil shape fixed taper ratio
Wroblewski & Ansell [51]	experimental	planar, unswept wing	minimum drag	**wingspan** **twist distribution**	fixed lift **fixed root bending moment, maneuver** fixed wing area fixed Reynolds number fixed airfoil shape fixed taper ratio
Lyu & Martins [52]	high fidelity	Blended Wing-Body	minimum drag	**wingspan** **twist distribution** airfoil shape angle of attack chord sweep angle structure thickness	steady level lift coefficient **max root bending moment** fixed taper ratio min internal volume fixed static margin fixed center of gravity trim

Table A3 Optimization summary and key constraints for studies including constraints related to the wing stress and stall.

	study type	*configuration*	*objective*	*key design variables*	*key constraints*
Phillips et al. [42]	analytic	planar, unswept rectangular wing	minimum induced drag	**wingspan** **lift distribution** wing weight	**max maneuver/hard-landing stress** **fixed stall speed** **fixed max lift coefficient**
van den Kieboom & Elham [53]	high fidelity	Fokker 100-class (similar)	minimum fuel weight	**wingspan** **flap deflection** airfoil shape chord distribution flap planform structure thickness	steady level lift coefficient **max stress, 2.5 g pull up** **max stress, -1.0 g push over** max fatigue stress, 1.3 g gust max stress, 1.0 g roll min aileron effectiveness **max takeoff distance** **min takeoff distance** fixed max takeoff weight

Table A4 Optimization summary and key constraints for studies including constraints related to the wing deflection and stall.

	study type	*configuration*	*objective*	*key design variables*	*key constraints*
Phillips et al. [42]	analytic	planar, unswept rectangular wing	minimum induced drag	**wingspan** **lift distribution** wing weight	**max maneuver/hard-landing deflection** **fixed stall speed** **fixed max lift coefficient**
Jansen et al. [46]	high fidelity	tapered, **elastic** wing with wingtip devices	maximum range	**wingspan** **jig twist** angle of attack root chord sweep angle dihedral distribution taper ratio structure thickness	steady level lift **max section lift coefficient (stall)** max stress, 2.5g maneuver
Mader et al. [60]	high fidelity	MIT D8 "double bubble" (**elastic**)	minimum fuel burn	**wingspan** **twist distribution** airfoil shapes angle of attack chord distribution tail rotation cruise altitude structure thickness structure design	steady level lift zero pitching moment (trim) max wingspan (gate constraint) **separation constraint (buffet)** min wing thickness min wing volume max yield stress, 2.5g/1g gust max buckling stress, 2.5g/-1g/1g gust structural thickness adjacency

Table A5 Optimization summary and key constraints for studies including constraints related to the wing stress and the wing loading.

	study type	*configuration*	*objective*	*key design variables*	*key constraints*
Phillips et al. [41,42]	analytic	planar, unswept rectangular wing	minimum induced drag	**wingspan** **lift distribution** wing weight [42]	**max maneuver/hard-landing stress** **fixed wing loading** fixed gross weight [41]
Taylor & Hunsaker [43]	analytic	planar, unswept tapered wing	minimum induced drag	**wingspan** **lift distribution** wing weight	**max maneuver/hard-landing stress** **fixed wing loading**
Löbert [40]	analytic	planar, unswept wing	minimum induced drag	**wingspan** **lift distribution**	**fixed wing area** fixed airfoil thickness **fixed gross weight** **max integrated moment/thickness ratio**
Stewart & Hunsaker [61]	multi fidelity	planar, unswept rectangular wing	minimum drag	**wingspan** **twist distribution**	**max maneuver/hard-landing stress** max maneuver/hard-landing deflection **fixed wing area** **fixed wing-structure weight**
McGeer [54]	multi fidelity	planar, unswept wing (light, low-speed)	minimum drag	**wingspan** **lift distribution** airfoil thickness	max section lift coefficient (stall) fixed parasitic drag coefficient **fixed wing-structure weight** **fixed wing area**
Ning & Kroo [57]	high fidelity	swept, planar trapezoidal wing	minimum drag	**wingspan** **cruise twist** **maneuver twist** chord distribution	min cruise/maneuver lift max section lift coefficient (inactive) **fixed wetted area** **max maneuver stress**
Piperni et al. [55]	high fidelity	large business jet	minimum cash operating cost	**aspect ratio** **lift distribution** airfoil shapes break chords sweep angle structure thickness	relative inboard/outboard sweep max/min strain fixed flight condition **max critical maneuver load** **fixed wing area** **fixed max takeoff weight**
Elham & van Tooren [58]	high fidelity	Airbus A320 (similar)	minimum fuel weight	**wingspan** **twist (2 locations)** airfoil shapes root chord sweep angle taper ratio structure thickness	steady level lift coefficient **max stress, 2.5 g pull up** **max stress, -1.0 g push over** max fatigue stress, 1.3 g gust max stress, 1.0 g roll **fixed max takeoff weight** **max wing loading**
Liem et al. [56]	high fidelity	Common Research Model	minimum fuel burn	**wingspan** **twist distribution** airfoil shapes angle of attack chord distribution sweep angle tail rotation	**min wing area** min wing-box volume fixed mean aerodynamic chord fixed center of gravity **fixed cruise/maneuver lift** **max maneuver stress** max gust stress

Table A6 Optimization summary and key constraints for studies including constraints related to the wing deflection and the wing loading.

	study type	*configuration*	*objective*	*key design variables*	*key constraints*
Phillips et al. [41,42]	analytic	planar, unswept rectangular wing	minimum induced drag	**wingspan** **lift distribution** wing weight [42]	**max maneuver/hard-landing deflection** **fixed wing loading** fixed gross weight [41]
McGeer [54]	multi fidelity	swept, **elastic** wing (light, high-speed)	minimum drag	**wingspan** **lift distribution** airfoil thickness	max integrated moment/thickness ratio max section lift coefficient (stall) fixed crest-critical Mach number **fixed wing area** **fixed wing-structure weight**
Kenway et al. [59]	high fidelity	undeflected Common Research Model (**elastic**)	minimum fuel burn	**wingspan** **twist distribution** airfoil shapes angle of attack chord length sweep angle altitude structure dimensions structure location	steady level lift coefficient max buffet lift coefficient structural thickness adjacency **fixed wing area** min fuel volume max yield stress, 2.5 g maneuver max yield stress, -1.0 g push over max buckling stress

Acknowledgements

This material is partially based upon work supported by NASA under Grant No. 80NSSC18K1696 issued by the Aeronautics Research Mission Directorate through the 2018 NASA Fellowship Activity with Nhan Nguyen as the NASA Technical Advisor.

References

[1] Phillips, W. F., "Lifting-Line Analysis for Twisted Wings and Washout-Optimized Wings," *Journal of Aircraft*, Vol. 41, No. 1, 2004, pp. 128–136. (doi:10.2514/1.262)

[2] Phillips, W. F., Fugal, S. R., and Spall, R. E., "Minimizing Induced Drag with Wing Twist, Computational-Fluid-Dynamics Validation," *Journal of Aircraft*, Vol. 43, No. 2, 2006, pp. 437–444. (doi:10.2514/1.15089)

[3] Gallay, S., and Laurendeau, E., "Preliminary-Design Aerodynamic Model for Complex Configurations Using Lifting-Line Coupling Algorithm," *Journal of Aircraft*, Vol. 53, No. 4, 2016, pp. 1145–1159. (doi:10.2514/1.C033460)

[4] Phillips, W. F., and Hunsaker, D. F., "Lifting-Line Predictions for Induced Drag and Lift in Ground Effect," *Journal of Aircraft*, Vol. 50, No. 4, 2013, pp. 1226–1233. (doi:10.2514/1.C032152)

[5] Wickenheiser, A., and Garcia, E., "Aerodynamic Modeling of Morphing Wings Using an Extended Lifting-Line Analysis," *Journal of Aircraft*, Vol. 44, No. 1, 2007, pp. 10–16. (doi:10.2514/1.18323)

[6] Phillips, W. F., and Snyder, D. O., "Modern Adaptation of Prandtl's Classic Lifting-Line Theory," *Journal of Aircraft*, Vol. 37, No. 4, 2000, pp. 662–670. (doi:10.2514/2.2649)

[7] Rasmussen, M. L., and Smith, D. E., "Lifting-Line Theory for Arbitrarily Shaped Wings," *Journal of Aircraft*, Vol. 36, No. 2, 1999, pp. 340–348. (doi:10.2514/2.2463)

[8] Bera, R. K., "Some remarks on the solution of the lifting line equation," *Journal of Aircraft*, Vol. 11, No. 10, 1974, pp. 647–648. (doi:10.2514/3.44397)
[9] Prandtl, L., "Tragflügel Theorie," *Nachricten von der Gesellschaft der Wissenschaften zu Göttingen*, Geschäeftliche Mitteilungen, Klasse, 1918, pp. 451–477.
[10] Prandtl, L., "Applications of Modern Hydrodynamics to Aeronautics," NACA TR-116, June 1921.
[11] Munk, M. M., "The Minimum Induced Drag of Aerofoils," NACA TR-12, 1923.
[12] Lundry, J. L., "Minimum Swept-Wing Induced Drag with Constraints on Lift and Pitching Moment," *Journal of Aircraft*, Vol. 4, 1967, pp. 73–74. (doi:10.2514/3.43797)
[13] Lissaman, P. B. S., and Lundry, J. L., "A Numerical Solution for the Minimum Induced Drag of Nonplanar Wings," *Journal of Aircraft*, Vol. 5, 1968, pp. 17–21. (doi:10.2514/3.43901)
[14] Ashenberg, J., and Weihsradius, D., "Minimum Induced Drag of Wings with Curved Planform," *Journal of Aircraft*, Vol. 21, 1984, pp. 89–91. (doi:10.2514/3.56733)
[15] Rokhsaz, K., "Effect of Viscous Drag on Optimum Spanwise Lift Distribution," *Journal of Aircraft*, Vol. 30, 1993, pp. 152–154. (doi:10.2514/3.46328)
[16] Demasi, L., "Induced Drag Minimization: A Variational Approach Using the Acceleration Potential," *Journal of Aircraft*, Vol. 43, 2006, pp. 669–680. (doi:10.2514/1.15982)
[17] Demasi, L., "Erratum on Induced Drag Minimization: A Variational Approach Using the Acceleration Potential," *Journal of Aircraft*, Vol. 43, 2006, p. 1247. (doi:10.2514/1.26648)
[18] Demasi, L., "Investigation on the Conditions of Minimum Induced Drag of Closed Wing Systems and C-Wings," *Journal of Aircraft*, Vol. 44, 2007, pp. 81–99. (doi:10.2514/1.21884)
[19] Demasi, L., Dipace, A., Monegato, G., and Cavallaro, R., "Invariant Formulation for the Minimum Induced Drag Conditions of Nonplanar Wing Systems," *AIAA Journal*, Vol. 52, 2014, pp. 2223–2240. (doi:10.2514/1.J052837)
[20] Demasi, L., Monegato, G., and Cavallaro, R., "Minimum Induced Drag Theorems for Multiwing Systems," *AIAA Journal*, Vol. 55, 2017, pp. 3266–3287. (doi:10.2514/1.J055652)
[21] Gray, W. L., and Schenk, K. M., "A Method for Calculating the Subsonic Steady-State Loading on an Airplane with a Wing of Arbitrary Planform and Stiffness," NACA TR-3030, December, 1953.
[22] Burdette, D. A., and Martins, J. R. R. A., "Impact of Morphing Trailing Edges on Mission Performance for the Common Research Model," *Journal of Aircraft*, Vol. 56, No. 1, 2019, pp. 369-384. (doi:10.2514/1.C034967)
[23] Kenway, G. K. W., and Martins, J. R. R. A., "Multipoint High-Fidelity Aerostructural Optimization of a Transport Aircraft Configuration," *Journal of Aircraft*, Vol. 51, No. 1, 2014, pp. 144-160. (doi:10.2514/1.C032150)
[24] James, K. A., Kennedy, G. J., and Martins, J. R. R. A., "Concurrent aerostructural topology optimization of a wing box," *Computers and Structures*, Vol. 134, 2014, pp. 1-17. (doi:10.1016/j.compstruc.2013.12.007)
[25] Mader, C. A., and Martins, J. R. R. A, "Stability-Constrained Aerodynamic Shape Optimization of Flying Wings," *Journal of Aircraft*, Vol. 50, No. 5, 2013, pp. 1431-1449. (doi:10.2514/1.C031956)
[26] Craig, A. P., and McLean, D. J., "Spanload Optimization for Strength Designed Lifting Surfaces," AIAA 88-2512, 6th Applied Aerodynamics Conference, Williamsburg, Virginia, 5–8 June 1988.
[27] Haftka, R. T., "Optimization of Flexible Wing Structures Subject to Strength and Induced Drag Constraints," *AIAA Journal*, Vol. 14, No. 8, 1977, pp. 1101–1106. (doi: 10.2514/3.7400)
[28] Grossman, B., Gurdal, Z., Strauch, G. J., Eppard, W. M., and Haftka, R. T., "Integrated Aerodynamic/Structural Design of a Sailplane Wing," *Journal of Aircraft*, Vol. 25, No. 9, 1988, pp. 855–860. (doi: 10.2514/3.45670)
[29] Wakayama, S., and Kroo, I. M., "Subsonic Wing Planform Design Using Multidisciplinary Optimization," *Journal of Aircraft*, Vol. 32, No. 4, 1995, pp. 746–753. (doi: 10.2514/3.46786)
[30] Calderon, D. E., Cooper, J. E., Lowenberg, M., and Neild, S. A., "On the Effect of Including Geometric Nonlinearity in the Sizing of a Wing," AIAA 2018-1680, 2018 AIAA/ASCE/AHS/ASC Structures, Structural Dynamics, and Materials Conference, Kissimmee, Florida, 8–12 January, 2018.
[31] Iglesias, S., and Mason, W. H., "Optimum Spanloads Incorporating Wing Structural Weight," AIAA 2001-5234, 1st Aircraft, Technology Integration, and Operations Forum, Los Angeles, California, 16–18 October 2001.
[32] Gopalarathnam, A., and Norris, R. K., "Ideal Lift Distributions and Flap Angles for Adaptive Wings," *Journal of Aircraft*, Vol. 46, No. 2, 2009, pp. 562–571. (doi: 10.2514/1.38713)
[33] Prandtl, L., "Über Tragflügel kleinsten induzierten Widerstandes," Zeitschrift für Flugtechnik und Motorluftschiffahrt, Vol. 24, No. 11, 1933, pp. 305–306.
[34] Jones, R. T., "The Spanwise Distribution of Lift for Minimum Induced Drag of Wings Having a Given Lift and a Given Bending Moment," NACA TR-2249, December 1950.

[35] Pate, D. J., and German, B. J., "Lift Distributions for Minimum Induced Drag with Generalized Bending Moment Constraints," *Journal of Aircraft*, Vol. 50, 2013, pp. 936–946. (doi:10.2514/1.C032074)
[36] DeYoung, J., "Minimization Theory of Induced Drag Subject to Constraint Conditions," NASA CR-3140, June 1979.
[37] Jones, R. T., and Lasinski, T. A., "Effect of Winglets on the Induced Drag of Ideal Wing Shapes," NASA TM-81230, Sept. 1980.
[38] Klein, A., and Viswanathan, S. P., "Minimum Induced Drag of Wings with Given Lift and Root-Bending Moment," *Zeitschrift fur Angewandte Mathematik und Physik*, Vol. 24, 1973, pp. 886–892.
[39] Klein, A., and Viswanathan, S. P., "Approximate Solution for Minimum Induced Drag of Wings with Given Structural Weight," *Journal of Aircraft*, Vol. 12, No. 2, 1975, pp. 124–126. (doi:10.2514/3.44425)
[40] Löbert, G., "Spanwise Lift Distribution for Forward- and Aft-Swept Wings in Comparison to the Optimum Distribution Form," *Journal of Aircraft*, Vol. 18, No. 6, 1981, pp. 496-498. (doi:10.2514/3.44717)
[41] Phillips, W. F., Hunsaker, D. F., and Joo, J. J., "Minimizing Induced Drag with Lift Distribution and Wingspan," *Journal of Aircraft*, Vol. 56, No. 2, 2019, pp. 431-441. (doi:10.2514/1.C035027)
[42] Phillips, W. F., Hunsaker, D. F., and Taylor, J. D., "Minimizing Induced Drag with Weight Distribution, Lift Distribution, Wingspan, and Wing-Structure Weight," AIAA 2019-3349, AIAA Aviation 2019 Forum, Dallas, Texas, 17-21 June 2019. (doi: 10.2514/6.2019-3349)
[43] Taylor, J. D., and Hunsaker, D. F., "Minimum Induced Drag for Tapered Wings Including Structural Constraints," *Journal of Aircraft*, Article in Advance. (doi:10.2514/1.C035757)
[44] Zhang, Z. J., "Exploratory High-Fidelity Aerostructural Optimization Using an Efficient Monolithic Solution Method," *PhD Thesis*, University of Toronto, 2017.
[45] Hoogervorst, J. E. K. and Elham, A., "Wing aerostructural optimization using the Individual Discipline Feasible Architecture," *Aerospace Science and Technology*, Vol. 65, 2017, pp. 90-99. (doi:10.1016/j.ast.2017.02.012)
[46] Jansen, P. W., Perez, R. E., and Martins, J. R. R. A., "Aerostructural Optimization of Nonplanar Lifting Surfaces," *Journal of Aircraft*, Vol. 47, No. 5, 2010, pp. 1490–1503. (doi: 10.2514/1.44727)
[47] Liem, R. P., Martins, J. R. R. A., and Kenway, G. K. W., "Expected drag minimization for aerodynamic design optimization based on aircraft operational data," *Aerospace Science and Technology*, Vol. 63, 2017, pp. 344-362. (doi:10.1016/j.ast.2017.01.006)
[48] Ting, E., Chaparro, D., Nguyen, N., and Fujiwara, G. E. C., "Optimization of Variable-Camber Continuous Trailing-Edge Flap Configuration for Drag Reduction," *Journal of Aircraft*, Vol. 55, No. 6, 2018, pp. 2217-2239. (doi:10.2514/1.C034810)
[49] Ranjan, P., "Computational Analysis of Planar Wings Designed for Optimum Span-Load," *MS Thesis*, University of Illinois at Urbana-Champaign, 2016.
[50] Verstraetan, J., G., and Slingerland, R., "Drag Characteristics for Optimally Span-Loaded Planar, Wingletted, and C Wings," *Journal of Aircraft*, Vol. 46, No. 3, May-June 2009, pp. 962-971. (doi:10.2515/1.39426)
[51] Wroblewski, G. E., and Ansell, P. J., "Prediction and Experimental Evaluation of Planar Wing Spanloads for Minimum Drag," *Journal of Aircraft*, Vol. 54, 2017, pp. 1664–1674. (doi:10.2514/1.C034156)
[52] Lyu, Z., and Martins, J. R. R. A., "Aerodynamic Design Optimization Studies of a Blended-Wing-Body Aircraft," *Journal of Aircraft*, Vol. 51, No. 5, September-October 2014, pp. 1604-1617. (doi:10.2514/1.C032491)
[53] van den Kieboom, K. T. H. and Elham, A., "Concurrent wing and high-lift system aerostructural optimization," *Structural and Multidisciplinary Optimization*, Vol. 57, No. 3, 2018, pp. 947-963. (doi:10.1007/s00158-017-1787-0)
[54] McGeer, T., "Wing Design for Minimum Drag with Practical Constraints," *Journal of Aircraft*, Vol. 21, 1984, pp. 879–886. (doi:10.2514/3.45058)
[55] Piperni, P., Abdo, M., Kafyeke, F., and Isikveren, A. T., "Preliminary Aerostructural Optimization of a Large Business Jet," *Journal of Aircraft*, Vol. 44, No. 5, September-October 2007, pp. 1422-1438. (doi:10.2514/1.26989)
[56] Liem, R. P., Kenway, G. K. W., and Martins, J. R. R. A., "Multimission Aircraft Fuel-Burn Minimization via Multipoint Aerostructural Optimization," *AIAA Journal*, Vol. 53, No. 1, January 2015, pp. 104-122. (doi:10.2514/1.J052940)
[57] Ning, S. A. and Kroo, I., "Multidisciplinary Considerations in the Design of Wings and Wing Tip Devices," *Journal of Aircraft*, Vol. 47, No. 2, March-April 2010, pp. 534-543. (doi:10.2514/1.41833)
[58] Elham, A. and van Tooren, M. J. L., "Coupled adjoint aerostructural wing optimization using quasi-three-dimensional aerodynamic analysis," *Structural and Multidisciplinary Optimization*, Vol. 54, No. 4, October 2016, pp. 889-906. (doi:10.1007/s00158-016-1447-9)
[59] Kenway, G. K. W., Martins, J. R. R. A., and Kennedy, G. J., "Aerostructural optimization of the Common Research Model configuration," AIAA 2014-3274, 15th AIAA/ISSMO Multidisciplinary Analysis and Optimization Conference, Atlanta, GA, 16-20 June 2014. (doi:10.2514/6.2014-3274)

[60] Mader, C. A., Kenway, G. K. W., Martins, J. R. R. A., Uranga, A., "Aerostructural Optimization of the D8 Wing with Varying Cruise Mach Numbers," AIAA 2017-4436, 18th AIAA/ISSMO Multidisciplinary Analysis and Optimization Conference, Denver, CO, 5-9 June 2017. (doi:10.2514/6.2017-4436)

[61] Stewart, A. J. and Hunsaker, D. F., "Minimization of Induced and Parasitic Drag on Variable-Camber Morphing Wings," AIAA 2020-0277, AIAA Scitech 2020 Forum, Orlando, FL, 6-10 January 2020. (doi:10.2514/6.2020-0277)

[62] Phillips, W. F. and Hunsaker, D. F., "Designing Wing Twist or Planform Distributions for Specified Lift Distributions," *Journal of Aircraft*, Vol. 56, No. 2, March-April 2019, pp. 847-849. (doi:10.2514/1.C035206)

[63] Phillips, W. F., "Aircraft Performance," *Mechanics of Flight*, 2nd ed., Wiley, Hoboken, NJ, 2010, pp. 259-376.